Proceedings of the ASME 2025
2025 ASME Pressure Vessels & Piping Conference
PVP2025
July 20–25, 2025, Montreal, QC

PVP2025-154876

VORTEX-INDUCED VIBRATION OF A RECTANGULAR CROSS SECTION WITH TRANSVERSE AND ROTATIONAL MODES

Mahmoud Shaaban[1,2,*], Mostafa R. Rashed[3], Atef Mohany[4]

[1]Mechanical Engineering Program, School of Engineering and Applied Sciences, Nile University, Giza, Egypt
[2]Smart Engineering Systems Center (SESC), Nile University, Giza, Egypt
[3]Mechanical Engineering Department, Faculty of Engineering, Modern University for Technology and Information, Cairo, Egypt
[4]Fluid-Structure Interaction and Noise Control Lab, Ontario Tech University, Oshawa, ON, Canada

ABSTRACT

Periodic vortex shedding downstream of a rectangular cross-section can result in excessive vibration, reducing fatigue life. Accurate characterization of the fluid-structural interaction can help develop models to predict the excitation of vibration at different flow velocities. These models can help develop methods to avoid the excitation of significant vibrations, ensuring structural integrity and preventing fatigue failure. In this work, the vibration response of a structure with a rectangular cross-section with an aspect ratio of 4 is numerically investigated when susceptible to both transverse and rotational vibration modes. A coupled two-dimensional fluid-structural model is used to solve the equations of structural vibration and fluid flow. The model provides predictions of the rectangular cross-section vibration under forces induced by vortex shedding. The amplitude, frequency, and phase characteristics of the coupled cross-flow and rotational modes are presented and compared to vortex-induced vibration in a single degree-of-freedom system. The coupling between modes at different flow velocities lock-in is investigated for cases where the two modes have equal or different natural frequencies. Although the two modes are structurally independent, results show that fluid forces introduce modal coupling if the two modal frequencies are equal, leading to elevated vibration levels away from the expected vortex-induced vibration lock-in range. However, this coupling effect did not materialize for cases where the two modal frequencies were not equal.

Keywords: vortex-induced vibration, computational fluid dynamics, fluid-structure interaction, rectangular cross-section, fatigue, structural integrity

*Corresponding author: mashaaban@nu.edu.eg

NOMENCLATURE

Symbols

D	characteristic length
F_y	transverse fluid force
f_n, $f_{n,y}$, $f_{n,r}$	modal frequency, transverse, rotational
f_v	vortex shedding frequency
k_y,k_r	stiffness: transverse, rotational
m	structure mass
m^*	mass ratio, $m/\rho V$
$\mathbf{n}$	unit vector normal to surface
I	cross-section moment of inertia per unit length
p	normalized pressure
Re	Reynolds number, $\rho UD/\mu$
St	Strouhal number, $f_v D/U$
t	time
T_z	fluid-induced torque
U, u	upstream flow velocity, normalized
U_r	reduced flow velocity, $U/f_n D$
V	volume
y, y_{rms}	transverse displacement, root mean square
θ, θ_{rms}	angular displacement, root mean square [degrees]
ϕ	phase angle [rad]
ζ	damping ratio
μ	fluid viscosity
ρ	fluid density

Abbreviations

CFD	Computational Fluid Dynamics
FSI	Fluid-Structure Interaction
GCI	Grid Convergence Index
RANS	Reynolds-Averaged Navier-Stokes
VIV	Vortex-Induced Vibration

Copyright © 2025 by ASME

1. INTRODUCTION

External flow over solid structures often results in vortex shedding that impacts the structures with periodic forces which depend on the cross-section geometry, incident flow angle, and flow velocity [1]. Structures with sufficient flexibility may respond with dynamic motion, leading to vortex-induced vibration [2]. Vortex-induced vibration has been under investigation for its significant applications in many engineering fields as extensively reviewed by several authors [3–5]. Vortex shedding occurs with a characteristic frequency f_v defined by the Strouhal number $St = f_v D/U$, dependent upon the characteristic length D, and the upstream flow velocity U. The Strouhal number St, in turn, is a function of the geometry and Reynolds number Re. On the other hand, the structural vibration occurs at modal frequencies that depend on its effective stiffness-to-inertia ratio and not on the reduced flow velocity $U_r = U/f_n D$, where f_n is the structural modal frequency. As the flow velocity increases from low values, the vortex shedding frequency and the associated dynamic force frequency on the structure approach the vibration modal frequency, resulting in a resonance-like condition. Consequently, the two frequencies become equal in a state of lock-in over a range of flow velocities, and significant vibration amplitudes are observed. This behavior results in high dynamic fluid forces on the structure as well as oscillating stresses, exacerbating vibration, and fatigue issues.

Structures of rectangular cross section can be subject to significant dynamic forces when subjected to fluid flow due to the dynamics of the vortex shedding process and its interaction with the structure [6, 7]. Significant research has focused on the transverse response of structures with a uniform solid cross-section under incident flow. In this mode of vibration, the cross section moves in a single direction normal to the flow direction. The observed vibration response depends on the mass ratio $m^* = m/\rho V$, a ratio of the structure mass m to the displaced fluid mass of density ρ and volume V , and the ratio ζ of the structural damping to its critical value. In addition to cylindrical structure, vortex-induced vibration of elastic slender structures was investigated. A few studies considered the flow-induced vibration of structures with a rectangular cross-section. Marra et al. [8] experimentally studied the vortex-induced vibrations of a rectangular cylinder with a streamwise length-to-height ratio of 4, developing a model to predict the vibration amplitude of similar structures. Daniels et al. [9] numerically studied the vortex-induced vibration of a rectangular cylinder, showing that the upstream turbulence levels can diminish the vibration amplitude. In addition to the transverse vibration observed for structures of circular cross-sections, rectangular structures may experience rotational vibration. Matsumoto et al. [10] experimentally studied the vortex-induced vibration of a rectangular cylinder of a cross-section aspect ratio of four, investigating torsional vibration modes around different centers of rotation. They identified two different types of vortex-induced excitation in both transverse and torsional motion, which are a shear layer instability related-vortex excitation, and Kármán vortex excitation.

While experimental investigations of vortex-induced vibration provide a high-fidelity source of data on the physical phenomena, the required setups tend to have a limited range of physical

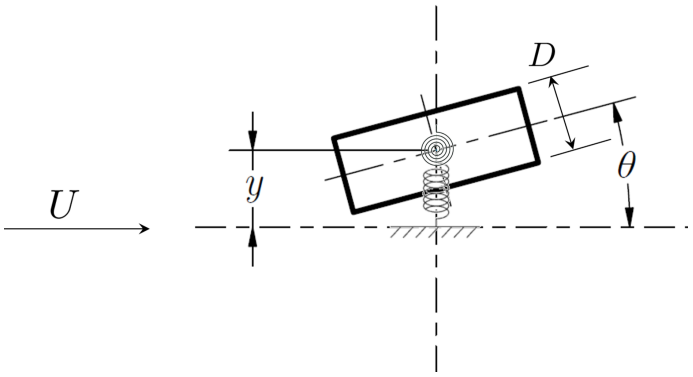


FIGURE 1: STRUCTURAL CONFIGURATION

configurations, including the geometric, size, mass parameters [11] . The study of vortex-induced vibration involves mathematical modeling that aims to provide predictions of the vibration amplitude and the flow field [12]. Computational fluid dynamic models have been used to provide high-fidelity predictions of the fluid-structure interaction, considering both the fluid and structure motion and resolving the interaction in physical time [13, 14]. Daniels et al. [9] used large eddy simulation to predict the flow-induced vibration of a rectangular cross-section with a side ratio of 4, representative of a bridge deck, for each rotational and cross-wind vibration mode.

While vortex-induced vibration of circular cylinders has been extensively analyzed, less detail is available for structures of rectangular cross sections that represent critical components such as supports, fins, and struts in many applications. Moreover, available studies often consider each vibration mode separately, although rotational and vibration modes are expected to interact if their natural frequencies are sufficiently close. This work aims to investigate the interaction between the rotational and transverse vibration modes of a structure with a rectangular cross-section of a streamwise to transverse side ratio of 4. The geometry and structural parameters are based on the experimental work of Matsumoto et al. [10] to provide an experimental basis for verification. The vibration response and flow field are investigated for two configurations, with a transverse to rotational modal frequency ratio of 1.0 and 0.65. A two-dimensional Reynolds-averaged Navier-Stokes equations model is fully coupled with a rigid-body motion structural solver to simulate the fluid-structure interaction. The observations in this article provide evidence of the dependency of the interaction and competition between the vibration mode on the frequency ratio, reduced flow velocity, and the vortex structure.

2. METHODOLOGY

2.1 Numerical model

A schematic of the model is shown in figure 2. The structure has a rectangular cross-section of transverse edge length D = 0.075 m and a streamwise edge length of 0.3 m. To resolve the fluid field and the associated forces affecting the structure, the compressible two-dimensional turbulent flow field around a rectangular cross-section is numerically modeled using Reynolds-Averaged Navier-Stokes (RANS) formulation at Reynolds num-

Copyright © 2025 by ASME

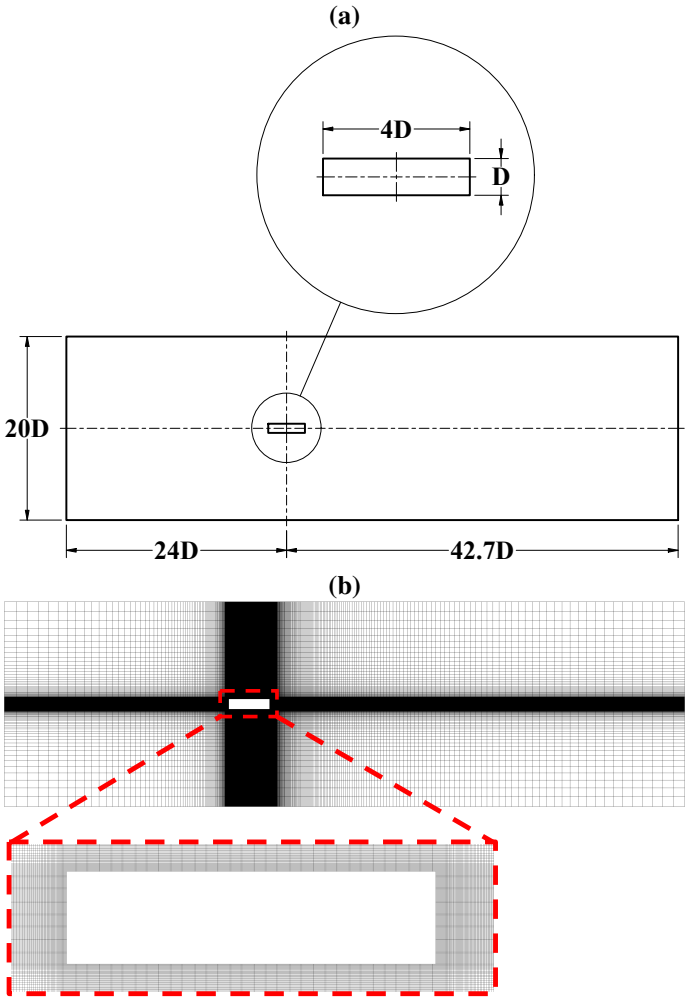


FIGURE 2: CONFIGURATION OF THE COMPUTATIONAL DOMAIN. (A) DOMAIN DIMENSIONS AND (B) COMPUTATIONAL GRID.

ber $Re = 4 \times 10^4$ based on the cross-section transverse thickness D and the upstream flow velocity at the vibration peak. The incompressible Navier–Stokes equations can be written as:

$$\nabla \cdot \mathbf{u} = 0 \tag{1}$$

$$\rho \frac{\partial \mathbf{u}}{\partial t} + \rho \left(\mathbf{u} \cdot \nabla \right) \mathbf{u} = -\nabla p + \mu \nabla^2 \mathbf{u} \tag{2}$$

The equations of motion of the structure are expressed as:

$$\begin{bmatrix} m & 0 \\ 0 & I \end{bmatrix} \begin{bmatrix} \ddot{y} \\ \ddot{\theta} \end{bmatrix} + \begin{bmatrix} k_y & 0 \\ 0 & k_r \end{bmatrix} \begin{bmatrix} y \\ \theta \end{bmatrix} = \begin{bmatrix} F_y \\ T_z \end{bmatrix} \tag{3}$$

where F_y and T_z are the fluid transverse force component and fluid-induced torque around the z axis, respectively. As equation 3 suggests, the two vibration modes are structurally independent. However, fluid forces are not independent and are dominated by the vortex shedding mechanism. Therefore, mode coupling may arise from the interaction of the fluid forces with the structure. Moreover, equation 3 includes no structural damping. Nevertheless, the added damping effect of the fluid viscous forces should limit the structural vibration. Consequently, the model would provide the upper limit of the vibration amplitude, as the structural vibration is expected to decrease with damping. Gravity is not included in the formulation of body forces for either the flow or the structure domain. The $k - \omega$ SST turbulence model is used to model the effect of turbulence on the flow field. The upstream flow is smooth and clear of perturbation at a zero incidence angle to the axis of the structure at its rotational neutral position. The structure is assumed to be sufficiently long and slender in the third dimension to ensure that forces are dominated by the two-dimensional flow and that end effects are marginal. The cross-section is constrained to move linearly only in the y direction, which is normal to the streamwise flow direction and normal to the z rotational axis. This mode of vibration, hereby referred to as transverse, is the typical heaving such that its driving force is the lift oscillating component. The two other possible translation components in the streamwise and axial directions are constrained through rigid fixation. The structure is expected to move under uniform structural stiffness over its length in the transverse direction.

TABLE 1: NUMERICAL MODEL BOUNDARY CONDITIONS.

Boundary	Pressure	Velocity
Inlet	$\nabla p \cdot \mathbf{n} = 0$	$\mathbf{u} = (U, 0)$
Domain sides	$\nabla p \cdot \mathbf{n} = 0$	$\mathbf{u} = (U, 0)$
Structure walls	$\nabla p \cdot \mathbf{n} = 0$	$\mathbf{u} = (0, 0)$
Outlet	$p = 0$	$\nabla(\mathbf{u} \cdot \mathbf{n}) = 0$

An iterative solver is implemented on the OpenFOAM finite volume open-source library. The iterative PISO solver iterates the pressure p and velocity $\mathbf{u}$ fields every time step to converge to absolute residuals of 10^{-6}. Second-order numerical discretization of the convection and flux terms is used to ensure stability and accuracy. A time step of 10^{-5} s is used at all flow velocities, resulting in a Courant number less than 1 for all cases, which provides an accurate resolution of the vibration cycle as well as the flow quantities. A structural motion solver is provided with the flow field quantities along with the centroid position and velocity from the previous time step . The iterative flow solver determines the pressure field around the structure and provides the updated flow field as an output. The structural solver calculates the stiffness and inertia forces applied on the cross sections and updates their velocity and location for use in the next time step. The process continues until a statistically steady oscillating behavior is observed for sufficient time to enable the calculation of the spectral domain, typically after 5 seconds. The structural frequency is calculated via a power spectral density analysis of the motion of the center of rotation, while the vortex shedding frequency f_v is calculated as the oscillating frequency of the lift force signal.

The model is used to predict the vibration response of a structure with a uniform rectangular cross-section and an aspect ratio of 4, where the longer edge is aligned in the streamwise direction. The object is allowed to rotate around its out-of-plane axis with a torsional spring with a linear stiffness coefficient of 272 N.m/rad with an angular moment of inertia of 0.01494 kg.m and no structural damping. The structural frequency of the rota-

Copyright © 2025 by ASME

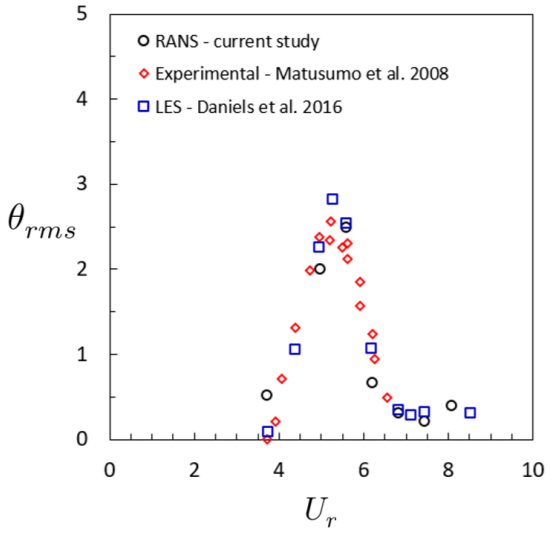


FIGURE 3: ROTATIONAL VIBRATION RESPONSE OF A RECTANGULAR CROSS-SECTION WITH A STREAMWISE TO TRANSVERSE ASPECT RATIO OF 4 AND A STRUCTURAL ROTATIONAL NATURAL FREQUENCY OF 21.5 HZ.

tional vibration is $f_{n,r}$ = 21.5 Hz. Two cases were considered for the transverse vibration, both with the same linear mass of 6.085 kg/m. In the first case, the natural frequency of the transverse motion was set equal to the rotational vibration mode at 21.5 Hz, by setting the stiffness to 111 kN/m. In the other case, the stiffness was set to 43.275 kN/m such that the peak of transverse vibration occurs at the same reduced velocity U_r = 5, based on the observations from the reference work of Daniels et al. [9]. In this case, the natural frequency of the transverse motion was set at $f_{n,y}$ = 13.3 Hz. The effect of these two configurations is presented in the following section.

2.2 Model validation

The spatial convergence of the mesh was evaluated using the Grid Convergence Index (GCI) method [15–17]. The GCI provides a quantitative assessment of the uncertainty related to mesh convergence, reflecting the percentage of error between the computed and asymptotic numerical values [18]. To evaluate the GCI, three mesh configurations, M1, M2, and M3, as detailed in Table 2, were used with a refinement ratio of r_{21} = 1.4. The GCI study indicated that the M2 mesh configuration produced good results with a negligible relative error of less than 3% and a grid convergence index of GCI_{21}= 1.4% .

Figure 3 shows the model prediction for the case of pure rotational motion compared with the prediction of two other studies for the same geometry in figure 1, namely the experimental study of Matsumoto et al. [10] and the Large Eddy Simulation by Daniels et al. [9]. The model prediction provides a good agreement with the results of both studies, falling within the same range and capturing the increasing and falling vibration amplitude trends within the lock-in range between U_r = 4 and U_r = 7. The agreement shows that the model can be reliably used to predict the vibration amplitude of this structural configuration.

TABLE 2: MESH SENSITIVITY ANALYSIS FOR A RECTANGULAR CROSS-SECTION OF D = 0.075 m, B = 0.3 m, AND UPSTREAM FLOW VELOCITY OF U_∞ = 9 m/s

Mesh	Number of elements	θ_{rms} [°]
M1	54,350	2.4493
M2	100,000	2.7067
M3	204,000	2.7903

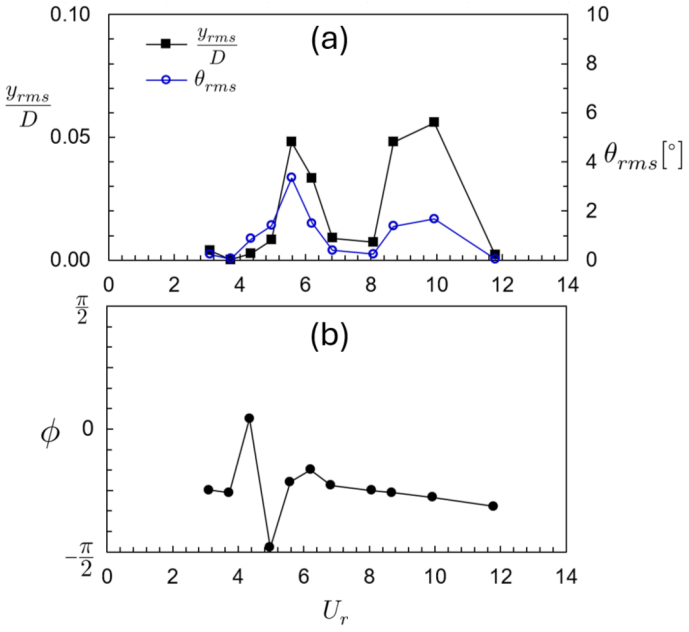


FIGURE 4: SIMULTANOUS TRANSVERSE AND ROTATIONAL VIBRATION RESPONSE OF A RECTANGULAR CROSS-SECTION WITH A STREAMWISE TO TRANSVERSE ASPECT RATIO OF 4 FOR EQUAL ROTATIONAL AND TRANSVERSE NATURAL FREQUENCIES OF f_n = 21.5 HZ. (A) ROOT MEAN SQUARE VIBRATION DISPLACEMENT AND ROTATION ANGLE AND (B) PHASE BETWEEN TRANSVERSE AND ROTATIONAL VIBRATION AT THE DOMINANT STRUCTURAL FREQUENCY f_n = 21.5 HZ.

3. RESULTS

Figure 4 shows the vibration response of the case where both the rotational and transverse vibration have the same natural frequency of $f_{n,r} = f_n, y$ = 21.5 Hz. Note that the reduced velocity for both modes is referenced to the same natural frequency of the rotational mode $f_{n,r}$ = 21.5 Hz. In figure 4a, the root mean square of the rotation angle and the transverse displacement are presented. The two modes were observed for all studied cases, vibrating at the same natural structural frequency expected, at 21.5 Hz for all cases. Evidently, the two modes interact together, such that two peaks of vibration are observed at the reduced flow velocities of U_r = 5, and U_r = 10. These two reduced velocities correspond to the conditions that give rise to the maximum vibration signal of the rotational mode and the transverse mode; respectively. Notably, each mode experiences elevated amplitudes of vibration when the other mode is under peak excitation. This suggests that the two modes exchange energy such that res-

Copyright © 2025 by ASME

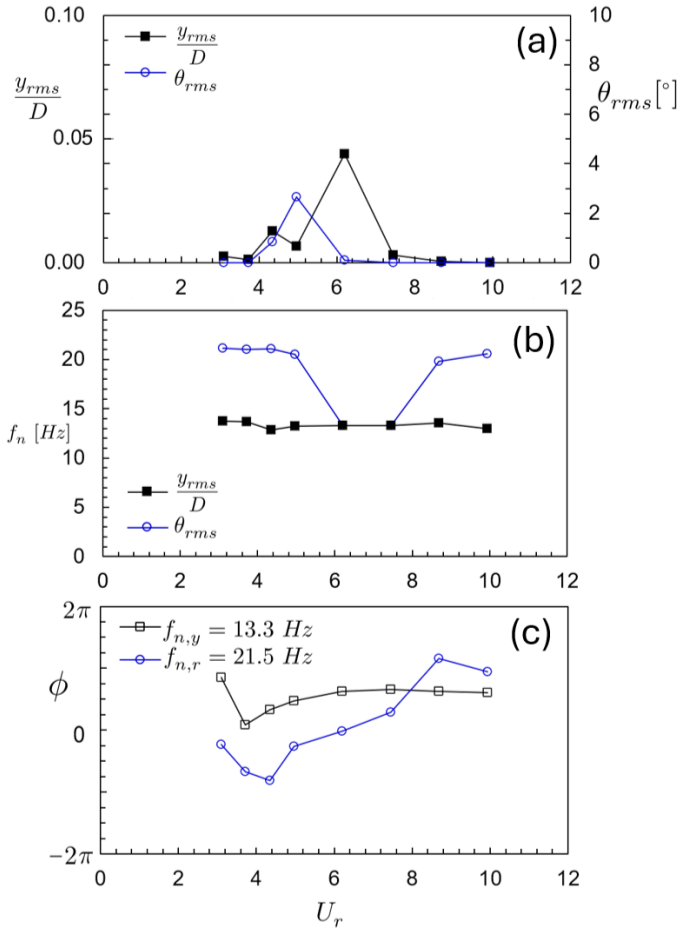


FIGURE 5: SIMULTANEOUS TRANSVERSE AND ROTATIONAL VIBRATION RESPONSE OF A RECTANGULAR CROSS-SECTION WITH A STREAMWISE TO TRANSVERSE ASPECT RATIO OF 4 FOR DIFFERENT NATURAL FREQUENCIES $f_{n,r}$ = 21.5 HZ AND $f_{n,y}$ = 13.3 HZ. (A) ROOT MEAN SQUARE VIBRATION DISPLACEMENT AND ROTATION ANGLE, (B) DOMINANT VIBRATION MODE FREQUENCY, AND (C) PHASE BETWEEN TRANSVERSE AND ROTATIONAL VIBRATION AT THE DOMINANT STRUCTURAL FREQUENCIES f_n = 21.5 HZ.

onance conditions of one vibration mode can lead to significant vibration of the other.

Figure 4b presents the phase between the two vibration modes, taking the rotational response as a reference. Therefore, positive values of the phase suggest a lead for the rotational vibration mode, and thus energy transfer from rotational to transverse vibration. It can be observed that the phase stays negative at nearly all reduced flow velocities. The only case where it flips to a positive value is at the peak of rotational vibration around U_r = 5.5. At this condition, the rotational mode dominates the motion and transfers energy to the transverse motion, leading to the elevated levels of vibration. As the reduced velocity increases, the phase reaches a significant negative value, signalling that the transverse motion dominates the coupled mode. This leads to energy transfer that elevates the levels of rotational motion where no vibration should be expected otherwise.

In figure 5, the vibration response of the coupled motion is shown for the case where $f_{n,r}$ = 21.5 Hz and $f_{n,y}$ = 13.3 Hz. Similar to the previous case in figure 5 the reduced velocity for both modes is referenced to the same natural frequency of the rotational mode $f_{n,r}$ = 21.5 Hz. Clearly, the difference in frequencies significantly affects the energy transfer between the two modes. The two vibration modes peak at different reduced velocities. The transverse vibration peak at U_r = 6.5, equivalent to a value of U_r = 10.5 if referenced to its own natural frequency, which is higher than its expected maximum vibration peak for an isolated transverse vibration mode. This behavior suggests that the coupled motion has an effect on the effective stiffness of the transverse mode. The rotational motion peaks at U_r = 5.5 similar to the previous case, which is the expected value for an isolated rotational vibration mode. The transverse motion seems to have a slight pickup in amplitude at U_r = 4.5. Still, the rotational motion did not pick up any significant levels outside its expected range of vibration for an isolated rotating case.

Figure 5b presents the vibration frequency. While the rotational vibration amplitude did not increase during excitation of the transverse mode, the frequency of rotational vibration locked in to the transverse mode. The opposite effect did not materialize at earlier flow velocities, which could result from the particular flow interactions during the two different resonance cases. Figure 5c shows the phase of vibration at the two different structural frequencies, referenced to the rotational motion. At the frequency of the transverse structural mode at $f_{n,y}$ = 13.3 Hz, the phase is positive at all cases. During the range of reduced flow velocities that led to significant transverse vibration, the phase is nearly unchanged at $\pi/4$, signaling energy transfer to the rotational mode, explaining the frequency lock-in. However, this energy transfer did not result in significant rotational vibration, suggesting a possible increase in fluid damping by the vortex structures. On the other hand, the phase is negative at the frequency of 13.3 Hz, predicting that the transverse mode takes in energy from the rotational mode at low values of U_r. The value of the phase at 13.3 Hz gradually turns positive, but no associated increase in amplitude is observed.

Figure 6 shows the normalized vorticity fields at the maximum rotational angle during a vibration cycle for the case with $f_{n,r}$ = $f_{n,y}$ = 21.5 Hz at three reduced velocities. The figure shows that the vibration amplitude is associated with significant changes in the flow field. At U_r = 6 and U_r = 15, where no significant rotational or transverse vibration is observed, no vortex shedding is observed directly downstream of the slender cross-section of the structure. On the other hand, the case with significant rotational and transverse vibration amplitude U_r = 9 shows a distinctive pattern of vortex shedding. The vortex street is shed in a 2S pattern with two parallel streets in opposite directions. The shear layer separating the leading edges of the rectangular cross-section attaches into the side of the structure, exerting significant fluid forces that contribute to the significant vibrational motion.

Figure 7 shows the normalized vorticity fields at the maximum rotational angle during a vibration cycle for the case with $f_{n,y}$ = 13.3 Hz, $f_{n,r}$ = 21.5 Hz at three reduced velocities. The observed behavior is similar to that for the case of the matched

Copyright © 2025 by ASME

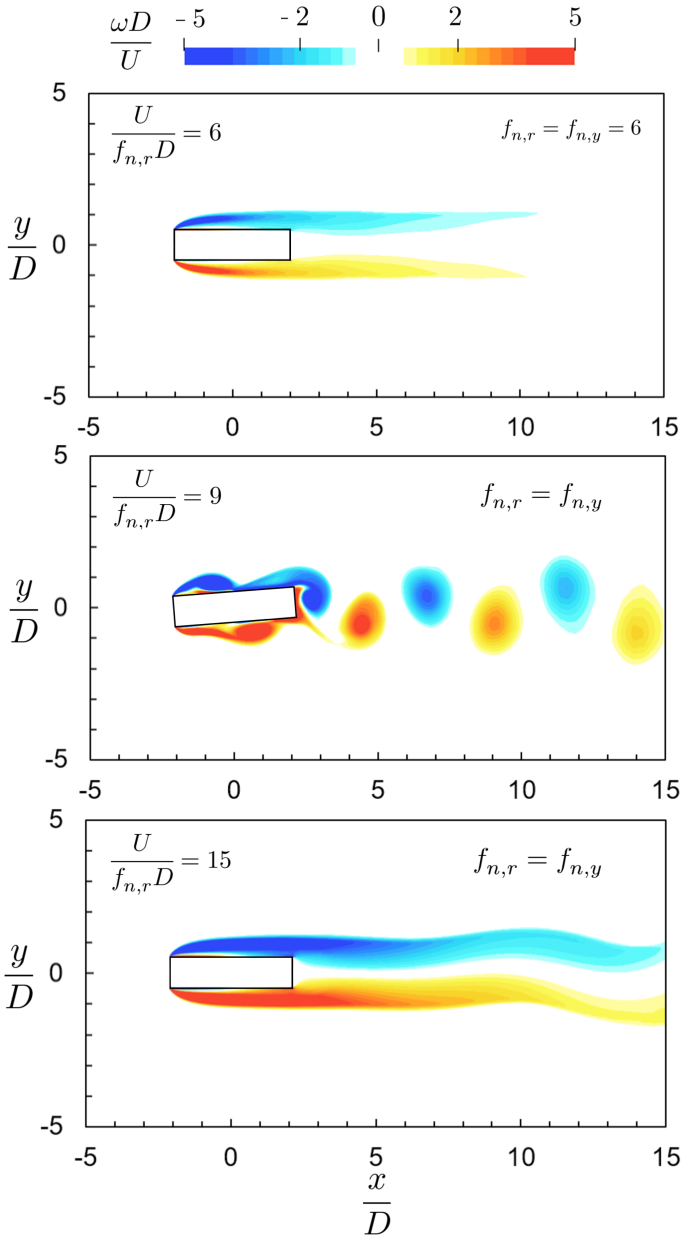


FIGURE 6: NORMALIZED VORTICITY FIELDS AT THE MAXIMUM ROTATIONAL ANGLE DURING A VIBRATION CYCLE FOR THE CASE WITH EQUAL ROTATIONAL AND TRANSVERSE VIBRATION FREQUENCIES AT THREE DIFFERENT REDUCED VELOCITIES.

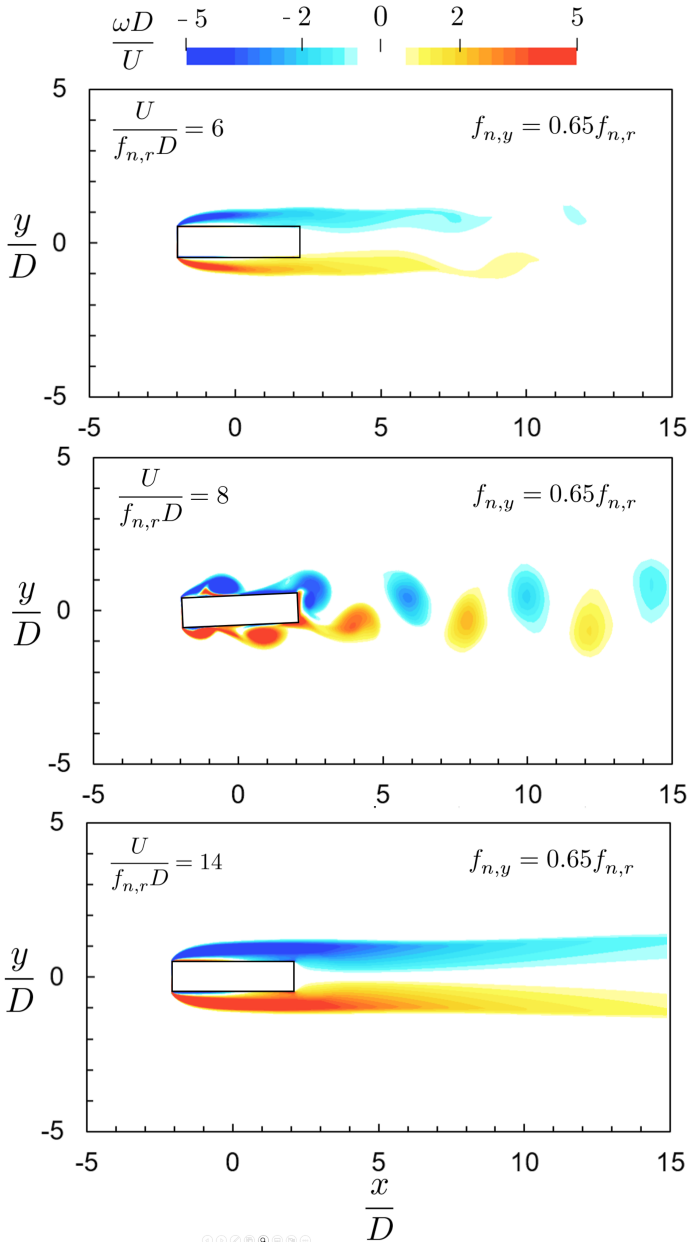


FIGURE 7: NORMALIZED VORTICITY FIELDS AT THE MAXIMUM ROTATIONAL ANGLE DURING A VIBRATION CYCLE FOR THE CASE WITH DIFFERENT ROTATIONAL AND TRANSVERSE VIBRATION FREQUENCIES AT THREE DIFFERENT REDUCED VELOCITIES.

frequency in Figure 6, indicating that the vibration amplitude is closely related to the flow field pattern. Reattachment of the shear layer and shedding into vortices is observed at the reduced velocity U_r = 8 at the peak of rotational vibration, while two parallel shear layers are observed for U_r = 6 and 14.

4. CONCLUSION

This study investigates the flow-excited vibration response of a structural rod with a uniform rectangular cross-section and a streamwise to transverse aspect ratio of 4. The structure is allowed to vibrate simultaneously in response to the fluid force in two directions: in rotation around its axis and linearly in the transverse direction normal to the streamwise direction. Two cases are considered to investigate the effect of the mismatch of the natural frequencies of the two modes. In one case, the two modes have the same free-vibration natural frequencies. In the other case, the two modes have different natural frequencies, so they are expected to peak at the same reduced flow velocity. A numerical model was used to predict the vibration response of the coupled motion by fully coupling the fluid force predictions of the Reynolds-averaged Navier-Stokes equations with the two-degree-of-freedom structural motion using a dynamic grid finite

Copyright © 2025 by ASME

volume method. Results show that the case with two modes having the same natural frequency leads to a strong coupling of the two modes, including a full frequency lock-in and energy exchange over a wide range of flow velocities. The two modes witness high levels of vibration over two different flow velocity ranges, with the rotational and transverse vibrations peaking at the expected values for each of them if isolated. On the other hand, when the two modes have a frequency ratio $f_{n,y}/f_{n,r} = 0.65$, this behavior is suppressed, and each mode is excited separately at a different flow velocity. In this case, the transverse vibration peak is delayed to a higher reduced flow velocity, preventing it from reaching significantly higher values. The flow field is closely related to the vibration response, where significant vibration vortex shedding is associated with vortex shedding and shear layer reattachment on the side of the structure, while cases with weak vibration did not show distinctive vortex shedding patterns.

These observations suggest that care should be taken when analyzing the vibration response of structures with similar vibration modes. Predictions of vibration provided by models that consider each of the modes separately may be erroneous or incomplete as they may miss early vibration episodes resulting from interaction of the modes. On the other hand, the mismatch between frequencies can lead to lower vibration amplitudes due to the effect of the two modes on the effective stiffness of each other. If carefully implemented and tested, an intended mismatch between the modal frequencies may be considered a tool to control the flow-excited vibration of the structure.

REFERENCES

[1] Matsumoto, M. "Vortex shedding of bluff bodies, a review." *Journal of Fluids and Structures* Vol. 13 No. 7–8 (1999): p. 791–811. DOI 10.1006/jfls.1999.0249.

[2] Williamson, C. and Govardhan, R. "vortex-induced vibrations." *Annual Review of Fluid Mechanics* Vol. 36 No. 1 (2004): p. 413–455. DOI 10.1146/annurev.fluid.36.050802.122128.

[3] Gao, D., Deng, Z., Yang, W. and Chen, W. "Review of the excitation mechanism and aerodynamic flow control of vortex-induced vibration of the main girder for long-span bridges: A vortex-dynamics approach." *Journal of Fluids and Structures* Vol. 105 (2021): p. 103348. DOI 10.1016/j.jfluidstructs.2021.103348.

[4] Duranay, A., Demirhan, A., Dobrucali, E. and Kinaci, O. "A review on vortex-induced vibrations in confined flows." *Ocean Engineering* Vol. 285 (2023): p. 115309. DOI 10.1016/j.oceaneng.2023.115309.

[5] Huera-Huarte, F. "Vortex-induced vibration of flexible cylinders in cross-flow." *Annual Review of Fluid Mechanics* (2024)DOI 10.1146/annurev-fluid-022724-014235.

[6] Shaaban, M. and Mohany, A. "Flow–acoustic coupling around rectangular rods of different aspect ratios and incidence angles." *Experiments in Fluids* Vol. 63 No. 2 (2022). DOI 10.1007/s00348-022-03380-2.

[7] Mohany, A., Shoukry, A. and Pastur, L. "Self-selection of flow instabilities by acoustic perturbations around rectangular cylinder in cross-flow." *Journal of Fluid Mechanics* Vol. 998 (2024): p. A51.

[8] Marra, A., Mannini, C. and Bartoli, G. "Measurements and improved model of vortex-induced vibration for an elongated rectangular cylinder." *Journal of Wind Engineering and Industrial Aerodynamics* Vol. 147 (2015): p. 358–367. DOI 10.1016/j.jweia.2015.08.007.

[9] Daniels, S., Castro, I. and Xie, Z. "Numerical analysis of freestream turbulence effects on the vortex-induced vibrations of a rectangular cylinder." *Journal of Wind Engineering and Industrial Aerodynamics* Vol. 153 (2016): p. 13–25. DOI 10.1016/j.jweia.2016.03.007.

[10] Matsumoto, M., Yagi, T., Tamaki, H. and Tsubota, T. "Vortex-induced vibration and its effect on torsional flutter instability in the case of B/D=4 rectangular cylinder." *Journal of Wind Engineering and Industrial Aerodynamics* Vol. 96 No. 6–7 (2008): p. 971–983. DOI 10.1016/j.jweia.2007.06.023.

[11] Francis, S. and Swain, A. "Modelling and harnessing energy from flow-induced vibration, particularly VIV and galloping: An explicit review." *Ocean Engineering* Vol. 312 (2024): p. 119290. DOI 10.1016/j.oceaneng.2024.119290.

[12] Wu, Y., C., Zhi, M., Ryley, Lien, F. and Yee, E. "Modelling of Flow-Induced Vibration of Bluff Bodies: A Comprehensive Survey and Future Prospects." *Energies* Vol. 15 No. 22 (2022): p. 8719. DOI 10.3390/en15228719.

[13] Zhang, Y., Cardiff, P. and Keenahan, J. "Wind-induced phenomena in long-span cable-supported bridges: a comparative review of wind tunnel tests and computational fluid dynamics modelling." *Applied Sciences* Vol. 11 No. 4 (2021): p. 1642. DOI 10.3390/app11041642.

[14] Shaaban, M. and Mohany, A. "Flow-induced vibration of three unevenly spaced in-line cylinders in cross-flow." *Journal of Fluids and Structures* Vol. 76 (2018): p. 367–383. DOI 10.1016/j.jfluidstructs.2017.10.007.

[15] Roache, P. "Quantification of uncertainty in computational fluid dynamics." *Annual Review of Fluid Mechanics* Vol. 29 No. 1 (1997): p. 123–160. DOI 10.1146/annurev.fluid.29.1.123.

[16] Rashed, Mostafa R., Elsayed, Mostafa E.A. and Shaaban, Mahmoud. "Influence of magnetically-induced nonlinear added stiffness on the lift galloping of square cylinders at low Reynolds number." *Journal of Fluids and Structures* Vol. 124 (2024): p. 104046. DOI 10.1016/j.jfluidstructs.2023.104046.

[17] Shaaban, M., Rashed, M. and Mohany, A. "Influence of resonant acoustic mode shape on source and sink patterns in the wake of a single cylinder based on Howe's energy corollary." *Volume 3: Fluid-Structure Interaction; High Pressure Technology*. 2024. American Society of Mechanical Engineers. DOI 10.1115/pvp2024-123184.

[18] Oberkampf, W. and Roy, C. *Verification and validation in scientific computing*. Cambridge University Press (2010). DOI 10.1017/cbo9780511760396.

Copyright © 2025 by ASME